

Agrinet: A Hyperspectral Image Based Precise Crop Classification Model

Aditi Palit^a, Himanshu Dolekar^b and Kalidas Yeturu^c

Department of Computer Science and Engineering, Indian Institute of Technology Tirupati, India

Keywords: Agriculture, Crop Classification, Hyperspectral Imagery, Convolution Neural Network.

Abstract: Modern smart agriculture utilizes Unmanned Aerial Vehicles (UAVs) with hyperspectral cameras to enhance crop production to address the food security challenges. These cameras provide detailed crop information for type identification, disease detection, and nutrient assessment. However, processing Hyper Spectral Image (HSI) is complex due to challenges such as high inter-class similarity, intra-class variability, and overlapping spectral profiles. Thus, we introduce the Agrinet model, a convolutional neural network architecture, to handle complex hyperspectral image processing. Our novelty lies in the image pre-processing step of selecting suitable bands for better classification. In tests, Agrinet achieved an impressive accuracy of 99.93% on the LongKou crop dataset, outperforming the existing methods in classification.

1 INTRODUCTION

According to the Food and Agricultural Organization of the United Nations (FAO), agriculture is vital in sustaining over 60% of the global population, utilizing approximately 12% of the world's land for farming activities (Bender, 2020). Thus, to feed such a big population, many advances are made in the agricultural sector by developed and developing countries. But despite significant progress in the field, challenges to food security persist (Rosegrant and Cline, 2003; Mc Carthy et al., 2018). These challenges include escalating demand for food, the strain on available land resources, the impact of climate change, diminishing pollination, outbreaks of plant diseases, water scarcity, inadequate food distribution systems (Calicioglu et al., 2019; Pereira, 2017).

Addressing these challenges requires immediate and proactive measures.

One notable technological advancement in this direction is the widespread use of drones (Veroustraete, 2015). With spectral cameras, drones can capture HSI that provides valuable insights into crops (Harakananavar et al., 2022; Mohanty and Salathé, 2016; Ahmed and Reddy, 2021). These HSI offer a range of applications, including crop type classification, early

disease detection, assessment of soil mineral and nutrient levels, identification of water stress in leaves, analysis of crop phenology, moisture content evaluation, and more (Khan et al., 2018; Ravikanth et al., 2017). Some models and pre-processing pipelines have been suggested in the literature to examine the HSI (Zhong et al., 2020a; Ramirez et al., 2020; Heble et al., 2018; Mogili and Deepak, 2018; Yamamoto et al., 2017; Guo et al., 2005; Xu et al., 2020), but compared to their performance, our model is better at selecting more meaningful spectral-spatial features. When classified, HSI presents challenges due to high inter-class similarity, spectral region overlap, and high intra-class variability.

As stated above, the classification of HSI presents three critical challenges that need to be addressed:

- **High Inter-Class Similarity.** Objects within an image often exhibit similar spectral reflectance properties, leading to overlapping spectral signatures. This similarity makes it challenging to distinguish between different crops or objects solely based on spectral profiles.
- **Overlapping Regions.** HSI suffers from the challenge of overlapping spectral signatures from different classes within the feature space. This overlap arises due to the limited number of spectral bands available.
- **High Intra-Class Variability.** The concept of high intra-class variability points to the phe-

^a  <https://orcid.org/0009-0007-7444-2994>

^b  <https://orcid.org/0009-0005-7487-1663>

^c  <https://orcid.org/0000-0002-9237-5453>

nomenon where various regions or sub-regions within a singular class exhibit dissimilar spectral signatures.

To address these challenges, we introduce the **Agrinet model**, a convolutional neural network with active band selection according to Normalized difference vegetation index (NDVI), for crop classification using UAV hyperspectral data. To facilitate incremental learning and prevent catastrophic forgetting, we decompose the multiclass classifier into a binary classifier (Singh et al., 2020) called **binary Agrinet**.

Normalized Difference Vegetation Index (NDVI): is a vegetation index that assesses vegetation by quantifying the disparity between near-infrared light, which vegetation reflects strongly, and red light, which vegetation absorbs. NDVI values consistently range from -1 to +1. Negative values typically indicate the presence of water, while values close to +1 suggest the presence of dense green foliage. Conversely, when NDVI is near zero, it indicates the absence of green leaves, potentially indicating an urbanized area. Thus, bands indicating vegetation are only chosen at the pre-processing step for the model to extract better spatial-spectral features.

Another aspect of the Agrinet model is that it doesn't adhere to an end-to-end convolutional architecture. The reason to refrain from using end-to-end convolutional models stems from a desire to prevent unwarranted model bulk. Implementing a separate pre-processing pipeline proves advantageous in crafting streamlined models, leading to a reduction in computational demands.

2 DATASET DESCRIPTION

HSI classification models often rely on low-resolution satellite datasets with limited labeled pixels. To overcome this, we used the WHU-Hi dataset (Luo et al., 2018), which consists of high-resolution UAV-borne HSI. This dataset comprises WHU-Hi-LongKou, WHU-Hi-HanChuan, and WHU-Hi-HongHu (Zhong et al., 2020b), offering improved spatial resolution. UAV datasets are better suited for crop classification, disease detection, and crop phenology profiling than satellite images.

3 AGRINET PIPELINE

Let us consider that we have HSI data of height(H) \times width(W) \times bands(B) along with the ground truth of

Table 1: Layer-based summary of Agrinet architecture.

Layer	Output Shape	No. of Parameters
Input Layer	(11,11,20,1)	0
Conv3D_1	(9,9,18,8)	224
Conv3D_2	(7,7,16,16)	3472
Conv3D_3	(5,5,14,32)	13856
Flatten	(11200)	0
Dense_1	(128)	1433728
Dropout_1	(128)	0
Dense_2	(64)	8256
Dropout_2	(64)	0
Output Layer	(No. of class)	1430

height(H) \times width(W). The dataset can be expressed as $X = [x_1, x_2, x_3 \dots x_B]^T \in HSI^{(H \times W \times B)}$. Thus, it has $H \times W$ samples associated with L class label per band based on the ground truth with collectively B bands (Ahmad et al., 2022). Each sample can be denoted as (x_i, y_j) where y_j is the label of sample x_i . Thus i^{th} sample belongs to j^{th} class.

The raw HSI data is preprocessed and band selection is applied based on the spectral profile by measuring the NDVI of the bands. Thus, no useful bands are clipped from the data. Feature extraction is done by incremental PCA, reducing the dataset's spectral dimensions. The HSI is divided into small 3D patches. These are divided into train-test sets to feed to the model to train the model and generate the classification map. Incremental principal component analysis is applied after band selection. The most significant N bands are chosen from B bands where $N \ll B$ while maintaining the spatial dimensions. For the HSI data cube to process with the Agrinet model (Figure1), the data cube has to be divided into small 3D overlapping spatial patches of a certain window size of S . Based on the 3D patches, ground labels are formed considering the central pixel. This creates the small K 3D HSI patches where $K \in HSI^{(S \times S \times N)}$ centered at location (m, n) covering $(S \times S)$ spatial window.

The input 3D HSI patches are convolved with a 3D kernel of the Agrinet model, thus calculating the dot product between the patches and kernel. The extracted features are subsequently subjected to the relu activation function, which introduces non-linearity to the learned representations. The activation value at position (a, b, c) in the i^{th} layer and j^{th} feature map is given by $u_{i,j}^{a,b,c}$.

$$\phi\left(\sum_{\delta=1}^{f_{i-1}} \sum_{r=-\alpha}^{\alpha} \sum_{s=-\beta}^{\beta} \sum_{t=-\lambda}^{\lambda} v_{i,j,\delta}^{r,s,t} * u_{(i-1),\delta}^{(a+r),(b+s),(c+t)} + b_{i,j}\right)$$

ϕ represents the activation function. f_{i-1} be the number of 3D feature map at $(i-1)^{th}$ layer. The depth of the kernel is represented by $v_{i,j}$ and $b_{i,j}$ corresponds to the bias term. To extract the spectral and spatial features, three convolutional 3D layers are deployed

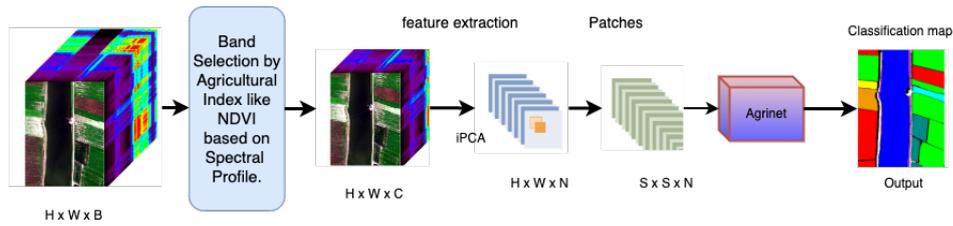


Figure 1: Proposed method Overview: The Agrinet model.

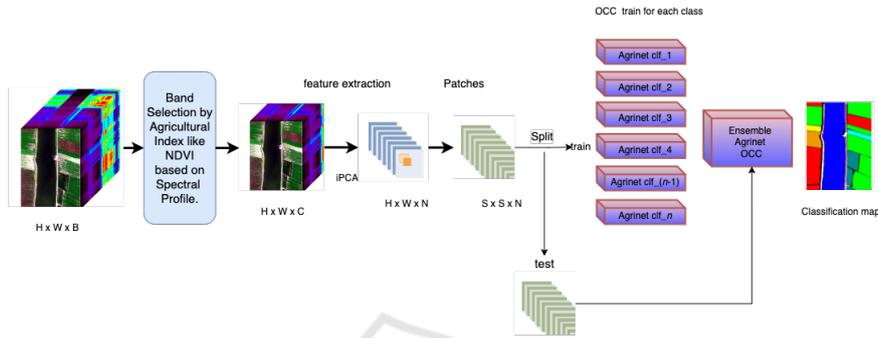


Figure 2: Binary Agrinet overview.

as shown in Figure1 so that the model can differentiate between the spectral band and spatial information without losing information. The weights are randomly initialized, and the Adam optimizer is used with the softmax function. The layer-based network summary is shown in Table 1.

4 BINARY AGRINET

By decomposing the multi-class crop classification into a binary classifier (Figure 2) for each crop and leveraging the one-versus-all strategy, the complexity and computational requirements are reduced, making it feasible to handle large-scale multi-class classification tasks effectively(Lorena et al., 2008).

The Agrinet binary model 2 has a sigmoid at the output layer, and a binary cross-entropy loss function is used. The individual classifier is optimized with an SGD optimizer. For binary Agrinet (Figure 2) only the training dataset is modified as per individual label classifier. On the training set, an individual binary classifier is built for each class label. Considering the interest class as the target class or positive class and other classes as the outlier class or negative class. This individual binary Agrinet model is trained and ensemble. The test set data is passed to ensembles of the binary Agrinet model, the probability score is calculated, and the maximum of them gives the final predicted class label.

Let n be the number of distinct classes in the

dataset D . let D_i and M_i be the dataset and binary classifier corresponding to label $i \in \{1 \dots n\}$ s.t. Now $\forall i \in 1 \dots n \exists$ a binary data set B_i corresponding to each D_i s.t

$$B_i = B_{i,p} \cup B_{i,n} \quad (1)$$

$$B_{i,p} = \{(x^j, I[y = i]) \mid x^j \in D \wedge I[y = i] = 1\} \quad (2)$$

$$B_{i,n} = \{(x^j, I[y = i]) \mid x^j \in D \wedge I[y = i] = 0\} \quad (3)$$

Let the training dataset for the i^{th} client be \tilde{D}_i where

$$\tilde{D}_i = B_{i,p} \cup B_{i,n} \quad (4)$$

$$M_i = \text{train}(\tilde{D}_i) \quad (5)$$

$x \in D_{test} \subseteq D$ and let ρ be the probability confidence function. Then, the predicted class for x is given by

$$\hat{y} = \arg \max_{i \in \{1 \dots n\}} \rho(M_i) \quad (6)$$

The sample is assigned to the class having the highest probability score.

5 EVALUATION ANALYSIS

To extract patches in the HSI cube, a window size of 15×15 is used. Meanwhile, the learning rate is fixed at 0.001 throughout the experiments. A total of 30 of the most significant bands are used after the band selection based on agricultural indices like the normalized difference vegetation index (NDVI) and moisture index using incremental principal component analysis. The size of the training set is 60%, the test data

Table 2: Performnace of Agrinet on comparison to benchmark models.

Dataset	Metric	SVM	FNEA-OO	SVRFMC	SSAN	SSRN	pResNet	CNNCRF	SSFCN	FPGA	CNN	Agrinet
LongKou	OA(%)	94.96	98.59	98.37	94.44	99.02	98.70	98.91	94.60	99.17	97.30	99.93
	AA(%)	95.18	97.48	97.41	95.38	99.39	98.88	98.21	95.27	99.30	97.40	99.76
	(κ)	0.9345	0.9815	0.9786	0.9279	0.9871	0.9830	0.9857	0.9300	0.9912	0.9647	0.9995
HanChan	OA(%)	73.55	88.83	89.86	87.34	91.29	95.32	93.74	94.26	97.45	93.74	99.75
	AA(%)	73.46	83.21	84.37	88.25	90.09	92.91	92.69	86.42	97.88	84.93	99.50
	(κ)	0.7414	0.8330	0.8435	0.8673	0.8815	0.9212	0.9290	0.8742	0.9747	0.8497	0.9969
HongHu	OA(%)	77.61	85.63	86.53	88.63	89.82	93.32	93.95	89.75	97.83	93.95	99.73
	AA(%)	71.23	83.13	87.16	84.93	91.68	95.83	94.78	92.03	97.79	86.16	99.31
	(κ)	0.6805	0.8590	0.8728	0.8415	0.8910	0.9412	0.9217	0.9219	0.9678	0.8210	0.9969

is 40%, and the validation is 30% of the training data (Ahmad et al., 2022).

For binary, an Agrinet window size of 11×11 is used to extract patches in the hyperspectral image cube. A total of 20 most significant bands are used after the band selection based on agricultural indices like NDVI and moisture index using incremental principal component analysis.

5.0.1 Analysis on WHU-Hi- LongKou Dataset

For evaluation purposes, we calculate overall accuracy (OA), kappa (κ) coefficient, and average accuracy (AA) using the confusion matrix obtained from the assessment. The metric of average accuracy (AA) provides insight into the classification performance per class. κ coefficient, on the other hand, serves as a statistical measure that gauges the level of agreement between the classification map and the ground truth map, relying on mutual information. The accuracy of Agrinet is compared with outcomes obtained from models in (Zhong et al., 2020b), providing a comprehensive benchmark against existing techniques as shown in Table 2. Agrinet’s performance demonstrates a marginal percentage advantage over the current state-of-the-art model across OA, AA, and κ on the WHU-Hi-LongKou dataset.

We evaluate our binary Agrinet model on the WHU-Hi-LongKou dataset. The overall accuracy from our binary Agrinet model is **87.6%**, and the average accuracy is **97.53%**. While the model might exhibit lower performance in direct comparison to the multiclass classifier. In future we wish to show it’s advantage over multiclass model when a new class is added.

5.0.2 Analysis on WHU-Hi-HanChuan Dataset

The performance comparison of our Agrinet model on the HanChan is shown in Table 2. OA and AA of Agrinet exhibit an approximate 2% to 3% increase compared to FPGA, which stands out as the superior model among the comparative approaches. The Agrinet model performs well in this data, which is

in a more complex urban-rural setting. The disparity becomes more pronounced in the case of the kappa value, with Agrinet showcasing an approximately 2% higher value.

5.0.3 Analysis on WHU-Hi-HongHu Dataset

As illustrated in Table 2, our model surpasses the performance of other models by a substantial margin on this dataset, which presents complexity due to its diverse crop labels within a single region and many class labels. In particular, Agrinet’s OA and AA scores are approximately 4% to 5% higher than most of the models, which stands as the leading comparative model. The most pronounced distinction is observed in the κ value, with Agrinet exhibiting an approximate 3% increase.

5.1 Conclusion and Future Work

Agrinet performs at a level on par with the state-of-the-art models and excels in all benchmark categories, including AA, OA, and κ . These results highlight Agrinet’s effectiveness, especially with complex datasets. However, it’s essential to acknowledge that our model’s high accuracy results from fully labeled, high-resolution training data, which may not reflect real-world conditions with incomplete labeling and lower spatial resolution. For future research, we plan to conduct in-depth ablation studies on the various hyperparameters of the models to gain a better understanding of their impact on model performance.

ACKNOWLEDGEMENTS

The authors acknowledge computational and funding support from the project numbered *CSE2122001FACEKALI* and titled *Design and Development of Disaster Response Dashboard for India* for carrying out the work.

REFERENCES

- Ahmad, M., Khan, A. M., Mazzara, M., Distefano, S., Ali, M., and Sarfraz, M. S. (2022). A fast and compact 3-d cnn for hyperspectral image classification. *IEEE Geoscience and Remote Sensing Letters*, 19:1–5.
- Ahmed, A. and Reddy, G. (2021). A mobile-based system for detecting plant leaf diseases using deep learning. *AgriEngineering*, 3:478–493.
- Bender, F. (2020). *Statistical methods for food and agriculture*. CRC Press.
- Calicioglu, O., Flammini, A., Bracco, S., Bellù, L., and Sims, R. (2019). The future challenges of food and agriculture: An integrated analysis of trends and solutions. *Sustainability*, 11(1):222.
- Guo, B. and Gunn, S., Damper, B., and Nelson, J. (2005). Adaptive band selection for hyperspectral image fusion using mutual information. " In *2005 7th International Conference on Information Fusion, IEEE*, 1.
- Harakannanavar, S., Rudagi, J., Puranikmath, V., Siddiqua, A., and Pramodhini, R. (2022). Plant leaf disease detection using computer vision and machine learning algorithms. *Global Transitions Proceedings*, 3:305–310. International Conference on Intelligent Engineering Approach(ICIEA-2022).
- Heble, S., Kumar, A., Prasad, K., Samirana, S. and Rajalakshmi, P., and Desai, U. (2018). A low power iot network for smart agriculture. In *2018 IEEE 4th World Forum on Internet of Things (WF-IoT)*, pages 609–614.
- Khan, M., Khan, H., Yousaf, A., Khurshid, K., and Abbas, A. (2018). Modern trends in hyperspectral image analysis: A review. *Ieee Access*, 6:14118–14129.
- Lorena, A., De Carvalho, A., and Gama, J. (2008). A review on the combination of binary classifiers in multiclass problems. *Artificial Intelligence Review*, 30:19–37.
- Luo, Y., Zou, J., Yao, C., Zhao, X., Li, T., and Bai, G. (2018). Hsi-cnn: A novel convolution neural network for hyperspectral image. In *2018 International Conference on Audio, Language and Image Processing (ICALIP)*, pages 464–469. IEEE.
- Mc Carthy, U., Uysal, I., Badia-Melis, R., Mercier, S., O'Donnell, C., and Ktenioudaki, A. (2018). Global food security—issues, challenges and technological solutions. *Trends in Food Science & Technology*, 77:11–20.
- Mogili, U. and Deepak, B. (2018). Review on application of drone systems in precision agriculture. *Procedia computer science*, 113:502–509.
- Mohanty, S.P. and Hughes, D. and Salathé, M. (2016). Using deep learning for image-based plant disease detection. *Frontiers in plant science*.
- Pereira, L. (2017). Water, agriculture and food: challenges and issues. *Water Resources Management*, 31(10):2985–2999.
- Ramirez, W., Achanccaray, P. and Mendoza, L., and Pacheco, M. (2020). Deep convolutional neural networks for weed detection in agricultural crops using optical aerial images. *IEEE Latin American GRSS & ISPRS Remote Sensing Conference (LAGIRS)*, pages 133–137.
- Ravikanth, L., Jayas, D., White, N., Fields, P., and Sun, D. (2017). Extraction of spectral information from hyperspectral data and application of hyperspectral imaging for food and agricultural products. *Food and bioprocess technology*, 10:1–33.
- Rosegrant, M. and Cline, S. (2003). Global food security: challenges and policies. *Science*, 302(5652):1917–1919.
- Singh, P., Singh, V., Pandey, M., and Karthikeyan, S. (2020). One-class classifier ensemble based enhanced semisupervised classification of hyperspectral remote sensing images. *2020 International Conference on Emerging Smart Computing and Informatics (ESCI)*, pages 22–27.
- Veroustraete, F. (2015). The rise of the drones in agriculture. *EC agriculture*, 2(2):325–327.
- Xu, B., Wang, W., Falzon, G., Kwan, P., Guo, L., Sun, Z., and Li, C. (2020). Livestock classification and counting in quadcopter aerial images using mask r-cnn. *International Journal of Remote Sensing*, 41(21):8121–8142.
- Yamamoto, K., Togami, T., and Yamaguchi, N. (2017). Super-resolution of plant disease images for the acceleration of image-based phenotyping and vigor diagnosis in agriculture. *Sensors*, 17(11):2557.
- Zhong, Y., Hu, X., Luo, C., Wang, X., Zhao, J., and Zhang, L. (2020a). Whu-hi: Uav-borne hyperspectral with high spatial resolution (h2) benchmark datasets and classifier for precise crop identification based on deep convolutional neural network with crf. *Remote Sensing of Environment*.
- Zhong, Y., Hu, X., Luo, C., Wang, X., Zhao, J., and Zhang, L. (2020b). Whu-hi: Uav-borne hyperspectral with high spatial resolution (h2) benchmark datasets and classifier for precise crop identification based on deep convolutional neural network with crf. *Remote Sensing of Environment*, 250:112012.